



# DNA binding, protein interaction, radical scavenging and cytotoxic activity of 2-oxo-1,2-dihydroquinoline-3-carbaldehyde(2'-hydroxybenzoyl)hydrazone and its Cu(II) complexes: A structure activity relationship study

Duraisamy Senthil Raja<sup>a</sup>, Nattamai S.P. Bhuvanesh<sup>b</sup>, Karuppannan Natarajan<sup>a,\*</sup>

<sup>a</sup> Department of Chemistry, Bharathiar University, Coimbatore 641046, Tamil Nadu, India

<sup>b</sup> Department of Chemistry, Texas A&M University, College Station, TX 77842, USA

## ARTICLE INFO

### Article history:

Received 19 July 2011

Received in revised form 16 December 2011

Accepted 21 December 2011

Available online 29 December 2011

### Keywords:

Copper(II) complexes

DNA binding

Protein binding

Antioxidant

Cytotoxicity

## ABSTRACT

Two new copper(II) complexes have been synthesized by reacting 2-oxo-1,2-dihydroquinoline-3-carbaldehyde(2'-hydroxybenzoyl)hydrazone (H<sub>2</sub>L) (**1**) with CuCl<sub>2</sub>·2H<sub>2</sub>O or Cu(NO<sub>3</sub>)<sub>2</sub>·3H<sub>2</sub>O, in order to obtain a clear picture on the role of counter ion in the biological properties of the complexes so obtained. Single-crystal X-ray diffraction studies revealed that both the complexes [CuCl(HL)(H<sub>2</sub>O)]·CH<sub>3</sub>OH (**2**) and [Cu(HL)(CH<sub>3</sub>OH)<sub>2</sub>]NO<sub>3</sub> (**3**) have square pyramidal geometry with the ligand coordinating through uni-negative tridentate ONO<sup>-</sup> fashion. The UV–Vis and fluorescence spectroscopy experimental evidences strongly suggested that the ligand and the two Cu(II) complexes could interact with calf thymus DNA (CT-DNA) through intercalation. The interactions of the compounds to bovine serum albumin (BSA) were investigated by UV–Vis, fluorescence and synchronous fluorescence spectra. The results indicated that all the three compounds could quench the intrinsic fluorescence of BSA in a static quenching way. Investigations of antioxidative properties showed that all the compounds have strong radical scavenging properties. Cytotoxic studies showed that the two copper(II) complexes exhibited effective cytotoxic activity against HeLa cancer cells. Overall, the complex **3** has exhibited better biological activity than that of the complex **2** and the ligand.

© 2011 Elsevier B.V. All rights reserved.

## 1. Introduction

Metal complexes have been widely applied in the field of medicine for centuries, although their molecular mechanism has not yet been entirely understood [1,2]. It is well known that metal ions present in the complexes are not only accelerating the drug action but also increase the effectiveness of the organic ligands [3]. The medicinal properties of metal complexes depend on the nature of the metal ions and the ligands [4]. The interest in preparation of new metal complexes has forced the study of the interaction of metal complexes with DNA and protein for their potential applications in biotechnology and medicine. Among the various interactions of metal complexes with DNA, intercalation is one of the most important DNA binding modes, which is related to the antitumor activity of the complex [5]. Moreover, the studies on interaction of protein with metal complexes can provide information of the structural features that determine the therapeutic effectiveness of the complex and have become an interesting field in recent years [6].

Copper with its bio-essential activity and oxidative nature has attracted numerous inorganic chemists to address Cu(II) complexes with medical applications [7–10]. Copper(II) complexes containing heterocyclic bases have been extensively explored in virtue of their strong interactions with DNA and cytotoxic activity [11–13]. In this connection, it is well known that hydrazones represent an important class of compounds in medicinal chemistry with great potential for chemotherapeutic applications [14,15]. Hence, it is important to know whether the Cu(II) complexes containing hydrazones can show different DNA binding, antioxidant and cytotoxic activities because of the inclusion of the copper(II) ion and also the effect of structural and electronic properties arising out of the coordination [16–18]. In this regard, copper(II) complexes containing 2-oxo-1,2-dihydroquinoline-3-carbaldehyde hydrazones have gained only a little attention [19,20].

Moreover, only a less attention has been in the study of the structure activity relationship of the complexes on their biological activity. In this line, we have recently reported that the copper(II) complexes derived from 2-oxo-1,2-dihydroquinoline-3-carbaldehyde N-substituted thiosemicarbazones and their structure activity relationship on biological properties such as protein binding, antioxidative and cytotoxic activity [21]. However, the structural and biological properties of hydrazone transition metal complexes derived from 2-oxo-1,2-

\* Corresponding author. Tel.: +91 422 2428319; fax: +91 422 2422387.

E-mail address: [k\\_natraj6@yahoo.com](mailto:k_natraj6@yahoo.com) (K. Natarajan).

dihydroquinoline-3-carbaldehyde have not been explored well. This aroused our interest in the synthesis of the ligand, 2-oxo-1,2-dihydroquinoline-3-carbaldehyde(2'-hydroxybenzoyl)hydrazone, and its copper(II) complexes with a view towards evaluating their structure activity relationship on biological properties such as DNA and protein binding, antioxidative and cytotoxic activity after the recent report of the reaction of 2-oxo-1,2-dihydroquinoline-3-carbaldehyde(2'-hydroxybenzoyl)hydrazone with  $\text{Cu}(\text{NO}_3)_2$  [20]. We carried out the same reaction and obtained a different complex for which the structure has been proved by single crystal X-ray studies. Moreover, no work seems to have been on  $\text{CuCl}_2$  with the above ligand. So here in, we report a comparative study of the biological properties of two new Cu(II) complexes synthesized from the same ligand with different Cu(II) salt namely chloride and nitrate, in order to have a correlation on the structure and activity.

## 2. Experimental

### 2.1. Materials/instrumentation

All starting precursors were of analytical grade, and double-distilled water was used throughout the experiments. 2-Oxo-1,2-dihydroquinoline-3-carbaldehyde was prepared according to the literature procedure [22]. The reagents and solvents were purchased commercially and used without further purification unless otherwise noted. Ethidium bromide (EB), calf thymus DNA (CT-DNA), bovine serum albumin (BSA) 2,2'-diphenyl-1-picrylhydrazyl (DPPH) and 3-(4,5-Dimethylthiazol-2-yl)-2,5-diphenyltetrazolium bromide (MTT) were purchased from Sigma-Aldrich and used as received. Elemental analyses (C, H, N) were performed on Vario EL III Elementar analyzer instrument. IR spectra ( $4000\text{--}400\text{ cm}^{-1}$ ) for KBr disks were recorded on a Nicolet Avatar Model FT-IR spectrophotometer.  $^1\text{H}$  NMR spectra were recorded on Bruker AMX 500 at 500 MHz using tetramethylsilane as an internal standard. Melting points were determined with a Lab India instrument. Electronic absorption spectra were recorded using Jasco V-630 spectrophotometer. Emission spectra were measured with Jasco FP 6600 spectrofluorometer. Solid state magnetic susceptibility measurements were carried out at room temperature on a Faraday balance calibrated using mercury(II) tetrathiocyanatocobaltate(II).

### 2.2. Preparation of compounds

#### 2.2.1. Synthesis of 2-oxo-1,2-dihydroquinoline-3-carbaldehyde(2'-hydroxybenzoyl)hydrazone ( $\text{H}_2\text{L}$ ) (**1**)

It was prepared with some modifications as described [20]. 2-hydroxybenzohydrazide (1.52 g, 0.01 mol) dissolved in warm methanol (50 mL) was added to a methanol solution (50 mL) containing 2-oxo-1,2-dihydroquinoline-3-carbaldehyde (1.73 g, 0.01 mol). The mixture was refluxed for an hour during which a yellow precipitate was formed. The reaction mixture was then cooled to room temperature and the solid compound formed was filtered. It was then washed with methanol and dried under vacuum. Yield, 93%. M.p. 315–317 °C. Elemental Anal. Calc. for  $\text{C}_{17}\text{H}_{13}\text{N}_3\text{O}_3$ : C, 66.72; H, 4.19; N, 13.71. Found: C, 66.44; H, 4.26; N, 13.67%. UV:  $\lambda_{\text{max}}$  (nm): 375. IR:  $\nu_{\text{max}}$  ( $\text{cm}^{-1}$ ):  $\nu_{\text{C=O}}$ : 1655,  $\nu_{\text{C=N}}$ : 1559.  $^1\text{H}$  NMR (DMSO- $d_6$  500 MHz, s, singlet; d, doublet; t, triplet; m, multiplet):  $\delta$  12.04 (s, 1H, O(4)H); 12.00 (s, 1H, N(3)H); 11.87 (s, 1H, N(2)H); 8.71 (s, 1H, C(1)H); 8.49 (s, 1H, C(6)H); 7.86–7.91 (m, 2H, C(7,10)H); 7.52–7.56 (t, 1H, C(9)H); 7.42–7.46 (t, 1H, C(8)H); 7.33–7.35 (d, 1H, C(17)H); 7.20–7.24 (t, 1H, C(16)H); 6.93–6.98 (m, 2H, C(14,15)H).

#### 2.2.2. Synthesis of the complex $[\text{CuCl}(\text{HL})(\text{H}_2\text{O})]\cdot\text{CH}_3\text{OH}$ (**2**)

A warm methanol solution (20 mL) containing  $\text{H}_2\text{L}$  (154 mg, 0.5 mmol) was added to a methanol solution (20 mL) of  $\text{CuCl}_2\cdot 2\text{H}_2\text{O}$  (85 mg, 0.5 mmol). The resulting greenish solution

was refluxed for 30 min. Green single crystals suitable for X-ray studies were obtained on slow evaporation. They were filtered off, washed with cold methanol, and dried under vacuum. Yield, 84%. M.p. 329–332 °C. Anal. Calc. for  $\text{C}_{18}\text{H}_{18}\text{ClCuN}_3\text{O}_5$ : C, 47.37; H, 3.91; N, 9.21. Found: C, 47.48; H, 3.98; N, 9.23%. UV:  $\lambda_{\text{max}}$  (nm): 369, 400, 421. IR:  $\nu_{\text{max}}$  ( $\text{cm}^{-1}$ ):  $\nu_{\text{C=O}}$ : 1629,  $\nu_{\text{C=N}}$ : 1586.  $\mu_{\text{eff}}$  (300 K): 1.76  $\mu_{\text{B}}$ .

#### 2.2.3. Synthesis of the complex $[\text{Cu}(\text{HL})(\text{CH}_3\text{OH})_2]\text{NO}_3$ (**3**)

It was prepared by the same procedure as described for **2** using  $\text{H}_2\text{L}$  (154 mg, 0.5 mmol) and  $\text{Cu}(\text{NO}_3)_2\cdot 3\text{H}_2\text{O}$  (121 mg, 0.5 mmol). Green single crystals were obtained. Yield, 82%. M.p. 331–334 °C. Elemental Anal. Calc. for  $\text{C}_{21}\text{H}_{21}\text{CuN}_5\text{O}_6$ : C, 50.07; H, 4.22; N, 13.87. Found: C, 50.15; H, 4.21; N, 13.92%. UV:  $\lambda_{\text{max}}$  (nm): 367, 400, 424. IR:  $\nu_{\text{max}}$  ( $\text{cm}^{-1}$ ):  $\nu_{\text{C=O}}$ : 1642,  $\nu_{\text{C=N}}$ : 1590.  $\mu_{\text{eff}}$  (300 K): 1.79  $\mu_{\text{B}}$ .

### 2.3. Crystallography

Single-crystal X-ray diffraction data of **2** and **3** were collected on BRUKER GADDS and BRUKER SMART 1000 X-ray (three-circle) diffractometers, respectively. Integrated intensity information for each reflection was obtained by reduction of the data frames with the program APEX2 [23]. The integration method employed a three dimensional profiling algorithm and all data were corrected for Lorentz and polarization factors, as well as for crystal decay effects with the program SAINT [23]. The structure was solved by direct methods using the program SHELXS-97 [24]. The refinement and all further calculations were carried out using SHELXL-97 [24]. The non-H atoms were refined anisotropically, using weighted full-matrix least-squares on  $F^2$ . In **3**, two molecules were found in the asymmetric unit and the absence of additional symmetry was confirmed using PLATON [25]. The hydrogen atoms bound to carbon were placed in idealized positions and refined using a riding model. Hydrogen atoms attached to N and O were located from difference Fourier maps and were set riding on the respective parent atom. Relevant data concerning data collection and details of the structure refinements are summarized in Table 1.

### 2.4. DNA interaction experiments

All the experiments involving the binding of compounds **1**, **2** and **3**, with CT-DNA were carried out in a doubly distilled water buffer with tris(hydroxymethyl)-aminomethane (Tris, 5 mM) and sodium chloride (50 mM) and adjusted to pH 7.2 with hydrochloric acid. A solution of CT-DNA in the buffer gave a ratio of UV absorbance of about 1.9 at 260 and 280 nm, indicating that the DNA was sufficiently free of protein. The DNA concentration per nucleotide was determined by absorption spectroscopy using the molar extinction coefficient value of  $6600\text{ dm}^3\text{ mol}^{-1}\text{ cm}^{-1}$  at 260 nm. The compounds were dissolved in a mixed solvent of 5% DMSO and 95% Tris-HCl buffer. Absorption titration experiments were performed with fixed concentrations of the compounds (25  $\mu\text{M}$ ) while gradually increasing the concentration of DNA (2.5–25  $\mu\text{M}$ ). While measuring the absorption spectra, an equal amount of DNA was added to both the test solution and the reference solution to eliminate the absorbance of DNA itself. The same experimental procedure was followed for emission studies also. The compound **1** and the compounds **2** and **3** were excited at 375 and 400 nm, respectively and their corresponding emission spectra were monitored at the range of 400–540 nm. EB-DNA experiments were conducted by adding the solution of the compounds to the Tris-HCl buffer of EB-DNA. The change of fluorescence intensity was recorded. The excitation and the emission wavelength were 515 nm and 602 nm, respectively.

**Table 1**  
Experimental data for crystallographic analyses.

	2	3
Empirical formula	C <sub>18</sub> H <sub>18</sub> ClCuN <sub>3</sub> O <sub>5</sub>	C <sub>19</sub> H <sub>20</sub> CuN <sub>4</sub> O <sub>8</sub>
Formula weight	455.34	495.93
T (K)	110(2)	293(2)
Wavelength (Å)	1.54178	0.71073
Crystal system	triclinic	triclinic
Space group	P $\bar{1}$	P $\bar{1}$
<i>Unit cell dimensions</i>		
a (Å)	8.4254(3)	10.792(17)
b (Å)	9.4613(4)	13.59(2)
c (Å)	12.7830(5)	16.66(3)
$\alpha$ (°)	71.314(3)	107.51(2)
$\beta$ (°)	71.855(2)	101.68(2)
$\gamma$ (°)	75.074(2)	104.705(19)
V (Å <sup>3</sup> )	903.08(6)	2148(6)
Z	2	4
Density (calc.) (Mg/m <sup>3</sup> )	1.675	1.533
Absorbance coefficient (mm <sup>-1</sup> )	3.406	1.070
F(000)	466	1020
Crystal size (mm <sup>3</sup> )	0.23 × 0.06 × 0.06	0.80 × 0.72 × 0.48
Index ranges	-8 ≤ h ≤ 9, -10 ≤ k ≤ 10, -14 ≤ l ≤ 14	-13 ≤ h ≤ 14, -17 ≤ k ≤ 17, -21 ≤ l ≤ 21
Number of observed reflections [I > 2σ(I)]	13,488	23,465
Independent reflections	2528 [R <sub>int</sub> = 0.0307]	9636 [R <sub>int</sub> = 0.0354]
Absorption correction	Semi-empirical from equivalents	Semi-empirical from equivalents
Maximum and minimum transmission	0.8217 and 0.5080	0.6276 and 0.4814
Refinement method	full-matrix least-squares on F <sup>2</sup>	full-matrix least-squares on F <sup>2</sup>
Data/restraints/parameters	2528/0/257	9636/0/577
Goodness-of-fit (GOF) on F <sup>2</sup>	1.070	1.039
Final R indices [I > 2σ(I)]	R <sub>1</sub> = 0.0296, wR <sub>2</sub> = 0.0797	R <sub>1</sub> = 0.0361, wR <sub>2</sub> = 0.0935
R indices (all data)	R <sub>1</sub> = 0.0346, wR <sub>2</sub> = 0.0814	R <sub>1</sub> = 0.0527, wR <sub>2</sub> = 0.1006

### 2.5. Protein binding studies

The excitation of BSA at 280 nm and the emission at 346 nm were monitored for the protein binding studies. The excitation and emission slit widths and scan rates were maintained constant for all the experiments. Samples were carefully degassed using pure nitrogen gas for 15 min. Quartz cells (4 × 1 × 1 cm) with high vacuum Teflon stopcocks were used for degassing. Stock solution of BSA was prepared in 50 mM phosphate buffer (pH 7.2) and stored in the dark at 4 °C for further use. Concentrated stock solution of compounds were prepared by dissolving the compounds in DMSO:phosphate buffer (1:50) and diluted suitably with phosphate buffer to required concentrations for all the experiments. Titrations were manually done by using micropipette for the addition of compounds. For synchronous fluorescence spectra also, the same concentration of BSA and compounds were used and the spectra were measured at two different  $\Delta\lambda$  (difference between the excitation and emission wavelengths of BSA) values such as 15 and 60 nm. If it is assumed that the binding of compounds with BSA occurs at equilibrium, the equilibrium binding constant can be analyzed according to the Scatchard equation:

$$\log[(I_0 - I)/I] = \log K_{\text{bin}} + n \log[Q] \quad (1)$$

Where  $I_0$  and  $I$  are the fluorescence intensities of the BSA in the absence and presence of compound;  $[Q]$  is the compound concentration;  $K_{\text{bin}}$  is the binding constant of compound with BSA and  $n$  is the number of binding sites. The value of  $K_{\text{bin}}$  can be determined from the slope of the plot of  $\log[(I_0 - I)/I]$  versus  $\log[Q]$ .

### 2.6. Antioxidant assays

The DPPH radical scavenging activity of the compounds was measured according to the method of Blois [26]. The DPPH radical is a stable free radical having  $\lambda_{\text{max}}$  at 517 nm. A fixed concentration

of the experimental compound ((1 mL; 5–100  $\mu\text{M}$ ) was added to solution of DPPH in methanol (125  $\mu\text{M}$ , 2 mL) and the final volume was made up to 4 mL with double distilled water. The solution was incubated at 37 °C for 30 min in dark. The decrease in absorbance of DPPH was measured at 517 nm.

The hydroxyl (OH) radical scavenging activities of the compounds have been investigated using the Nash method [27]. *In vitro* hydroxyl radicals were generated by Fe<sup>3+</sup>/ascorbic acid system. The detection of hydroxyl radicals was carried out by measuring the amount of formaldehyde formed from the oxidation reaction with DMSO. The formaldehyde produced was detected spectrophotometrically at 412 nm. A fixed concentration of the experimental compound (1 mL; 5–100  $\mu\text{M}$ ) was added to a mixture of 1.0 mL of iron-EDTA solution (0.13% ferrous ammonium sulfate and 0.26% EDTA), 0.5 mL of EDTA solution (0.018%), and 1.0 mL of DMSO (0.85% DMSO (v/v) in 0.1 M phosphate buffer, pH 7.4) were sequentially added in the test tubes. The reaction was initiated by adding 0.5 mL of ascorbic acid (0.22%) and incubated at 80–90 °C for 15 min in a water bath. After incubation, the reaction was terminated by the addition of 1.0 mL of ice-cold trichloroacetic acid (17.5% w/v). Subsequently, 3.0 mL of Nash reagent was added to each tube and left at room temperature for 15 min. The intensity of the color formed was measured spectrophotometrically at 412 nm against reagent blank.

Assay of nitric oxide (NO) scavenging activity is based on the method [28], where sodium nitroprusside in aqueous solution at physiological pH spontaneously generates nitric oxide, which interacts with oxygen to produce nitrite ions that can be estimated using Griess reagent. Scavengers of nitric oxide compete with oxygen leading to reduced production of nitrite ions. For the experiment, sodium nitroprusside (10 mM) in phosphate buffered saline was mixed with a fixed concentration of the compound (1 mL; 5–100  $\mu\text{M}$ ) and incubated at room temperature for 150 min. After the incubation period, 0.5 mL of Griess reagent

containing 1% sulfanilamide, 2% H<sub>3</sub>PO<sub>4</sub> and 0.1% N-(1-naphthyl) ethylenediaminedihydrochloride were added. The absorbance of the chromophore formed was measured at 546 nm.

The superoxide (O<sub>2</sub><sup>-</sup>) radical scavenging assay was based on the capacity of the compounds to inhibit formazan formation by scavenging the superoxide radicals generated in riboflavin-light-NBT system [29]. Each 3 mL reaction mixture contained 50 mM sodium phosphate buffer (pH 7.6), 20 µg riboflavin, 12 mM EDTA, 0.1 mg NBT and 1 mL experimental compound solution (5–100 µM). Reaction was started by illuminating the reaction mixture with different concentrations of complex for 90 s. Immediately after illumination, the absorbance was measured at 590 nm. The entire reaction assembly was enclosed in a box lined with aluminum foil. Identical tubes with reaction mixture kept in dark served as blanks.

For the above four assays, all the tests were run in triplicate and various concentrations of the compounds were used to fix a concentration at which compounds showed in and around 50% of activity. In addition, the percentage of activity was calculated using the formula, % of activity = [(A<sub>0</sub> - A<sub>c</sub>)/A<sub>0</sub>] × 100 (A<sub>0</sub> and A<sub>c</sub> are the absorbance in the absence and presence of the tested complex, respectively). The 50% of activity (IC<sub>50</sub>) can be calculated using the percentage of activity results.

### 2.7. Cytotoxicity assay

Cytotoxicity studies of the compounds and cisplatin were carried out on human cervical cancer cells (HeLa) and NIH 3T3 mouse embryonic fibroblasts which were obtained from National Centre for Cell Science, Pune, India. Cell viability was carried out using the MTT assay method. The HeLa cells were grown in Eagles minimum essential medium containing 10% fetal bovine serum (FBS). NIH 3T3 fibroblasts were grown in Dulbeccos Modified Eagles Medium (DMEM) containing with 10% FBS. For screening experiment, the cells were seeded into 96-well plates in 100 µL of respective medium containing 10% FBS, at plating density of 10,000 cells/well and incubated at 37 °C, 5% CO<sub>2</sub>, 95% air and 100% relative humidity for 24 h prior to addition of compounds. The compounds were dissolved in DMSO and diluted in respective medium containing 1% FBS. After 24 h, the medium was replaced with respective medium with 1% FBS containing the compounds at various concentration and incubated at 37 °C, 5% CO<sub>2</sub>, 95% air and 100% relative humidity for 48 h. Triplicate was maintained and the medium containing without the test compounds were served as control. After 48 h, 10 µL of MTT (5 mg/mL) in phosphate buffered saline (PBS) was added to each well and incubated at 37 °C for 4 h. The medium with MTT was then flicked off and the formed formazan crystals were dissolved in 100 µL of DMSO and then measured the absorbance at 570 nm using micro plate reader. The % of cell inhibition was determined using the following formula and graph was plotted between % of cell inhibition and concentration and from this IC<sub>50</sub> value was calculated. % inhibition = [mean OD of untreated cells (control)/mean OD of treated cells (control)] × 100.

## 3. Results and discussion

### 3.1. Synthesis and characterization

The synthetic routes of the ligand, 2-oxo-1,2-dihydroquinoline-3-carbaldehyde(2'-hydroxybenzoyl)hydrazone and its copper(II) complexes have been outlined in Scheme 1. The ligand was prepared by the condensation reaction of 2-oxo-1,2-dihydroquinoline-3-carbaldehyde with 2-hydroxybenzohydrazide in methanol. It was characterized by elemental analysis, IR, and <sup>1</sup>H-NMR spectroscopy. The assignments for IR and <sup>1</sup>H NMR spectra are given in the preparation section. The copper(II) complexes were prepared

by the direct reaction of the ligand with copper(II) salts in methanol. The single crystals of new copper(II) complexes were isolated by slow evaporation of the reaction mixture over a period of 30–35 days. The IR peak shift in ν<sub>C=O</sub> and ν<sub>C=N</sub> of the ligand in the complex gave an idea about its coordination to copper(II). The experimental μ<sub>eff</sub> values of 1.76 and 1.79 for **2** and **3** confirmed the +2 oxidation state of copper in the complexes. All the compounds are air stable for extended periods and remarkably soluble in methanol, ethanol, DMF and DMSO. Unlike **1** and **2**, the **3** is highly soluble in water. The structures of the new copper(II) complexes were determined by single crystal X-ray crystallographic studies.

### 3.2. X-ray structural characterization

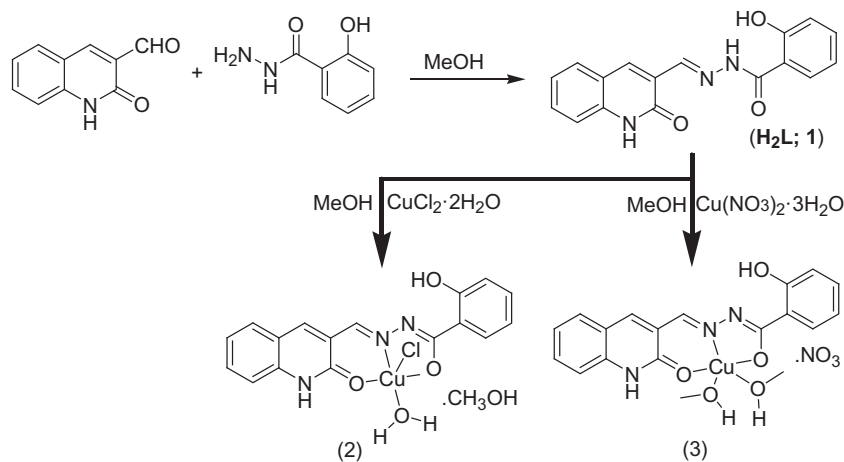
The ORTEP diagram of [CuCl(HL)(H<sub>2</sub>O)]·CH<sub>3</sub>OH is shown in Fig. 1. Important bond lengths and angles are summarized in Table 2. The complex contains a penta coordinated copper(II) ion coordinated with one ONO tridentate uni-negative ligand, one coordinated chloride ion and one water molecule along with one methanol molecule in the lattice. The copper(II) ion lies at about 0.238 Å above the average basal plane towards the axial O3 atom. The dihedral angle between the mean planes of the five-member chelate ring and the six-member one is 1.86°. Since the hydrazone moieties have both the hydrogen bond donors and the hydrogen bond acceptors, the species provide the possibility of forming hydrogen bonds in the crystal. In fact, the crystal lattice of the complex showed a two dimensional array in which each unit of the complex is hydrogen bonded to the other involving N2 and N3 nitrogen atoms and the O1, O2, O3, O4 and O20 oxygen atoms (Fig. S1, Supporting Information). The hydrogen bonding parameters for **2** have been given in Table S1 (Supporting Information).

An ORTEP view of the cationic complex [Cu(HL)(CH<sub>3</sub>OH)<sub>2</sub>]NO<sub>3</sub> is given in Fig. 2. The crystal structure consists of discrete [Cu(HL)(-CH<sub>3</sub>OH)<sub>2</sub>]<sup>+</sup> cations and nitrate anions. Five donor atoms in a square pyramidal fashion (4 + 1) surround the copper(II) ion in the complex. The basal plane is made up from the O, N, and O atoms of the tridentate uni-negative ligand and one oxygen atom of the methanol molecule, while the oxygen from another methanol molecule has taken the apical vertex. Cu(II) ion lies at 0.186 Å above the average basal plane towards the apical oxygen of methanol molecule. In addition, there is an appreciable Jahn–Teller effect highlighted by an axial Cu–O36 distance (2.262(4) Å) significantly longer than that observed for Cu–O35 distance (1.968(2) Å). The dihedral angle between the mean planes of the five member chelation ring and the six member one is 4.60° which ensures that the planarity of square should be appreciable. The molecular packing suggests that the stabilization of the lattice must have been due to several hydrogen bonds, mainly involving the N2, N3, O3, O35, O36 and O51 atoms (Fig. S2, Supporting Information). The hydrogen bonding parameters for **3** have been given in Table S2 (Supporting Information). It is to be noted that in the X-ray structural analysis, two crystallographically distinct molecules were found in the asymmetric unit but both have almost similar structural parameters (bond angle and bond length). So the structure of one of the molecule has been discussed above. Important bond lengths and angles for both the complexes are summarized in the Table 2 and they agree well with those found in related copper(II) complexes [19–21].

### 3.3. DNA binding studies

#### 3.3.1. Absorption spectroscopic studies

The application of electronic absorption spectroscopy is one of the most useful techniques for DNA-binding studies of small molecules [30]. The absorption spectra of the ligand (**1**), complexes **2** and **3** in the absence and presence of CT-DNA (at a constant



**Scheme 1.** The synthetic routes of the ligand and its Cu(II) complexes.

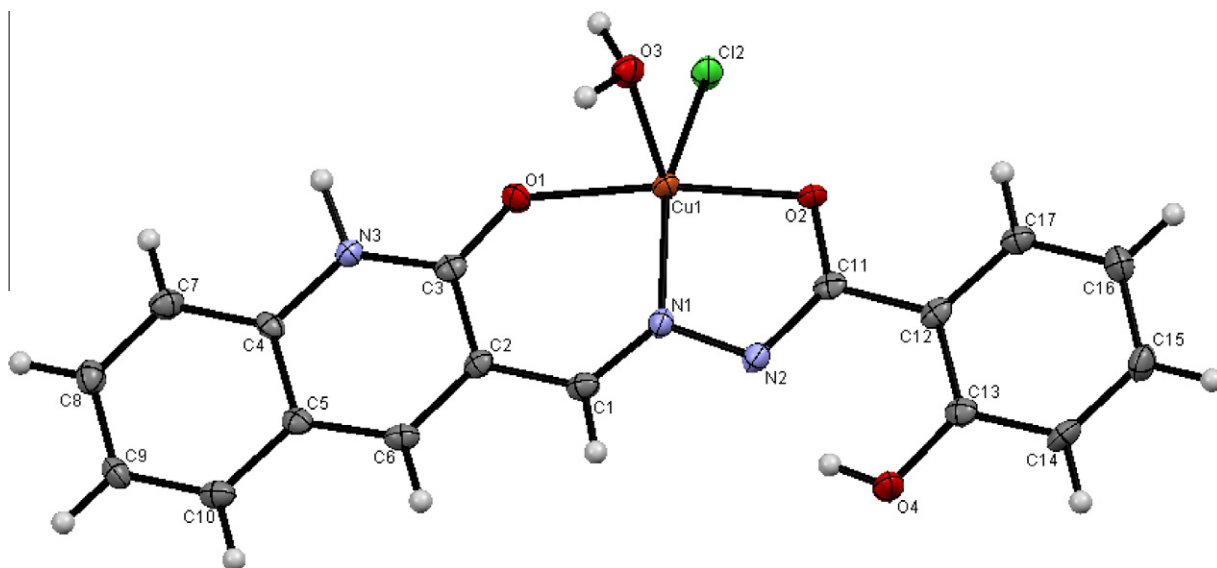


**Fig. 1.** ORTEP view of the molecular structure and atom-labeling scheme of **2**. Thermal ellipsoids are drawn at 50% probability level. The methanol molecule has been omitted for clarity.

concentration of compounds) are given in Fig. 3. In the presence of DNA, the absorption band of the ligand at about 375 nm exhibited hypochromism of about 17.91%. Complex **2** exhibited hypochromism of about 49.62%, 51.07% and 46.97% with red shift of about 1, 2 and 4 nm at 369, 400 and 421 nm, respectively. On the other hand, **3** exhibited hypochromism of about 51.32%, 53.09% and 52.61% with red shift of about 2, 1 and 3 nm at 367, 400 and 424 nm, respectively. These results suggested an intimate association of the compounds with CT-DNA and it is also likely that these compounds bind to the helix via intercalation [31]. After the compounds intercalate to the base pairs of DNA, the  $\pi^*$  orbital of the intercalated compounds could couple with  $\pi$  orbitals of the base pairs, thus decreasing the  $\pi \rightarrow \pi^*$  transition energies. Therefore, these interactions resulted in the observed hypochromism [32]. The complexes **2** and **3** showed more hypochromicity than the ligand, indicating that the binding strength of the copper(II) complexes are much stronger than that of the free ligand. In order to compare quantitatively the binding strength of the compounds, the intrinsic binding constants ( $K_b$ ) of them with CT-DNA were determined from the following equation [33],

$$[\text{DNA}]/(\varepsilon_a - \varepsilon_f) = [\text{DNA}]/(\varepsilon_b - \varepsilon_f) + 1/K_b(\varepsilon_b - \varepsilon_f) \quad (2)$$

where [DNA] is the concentration of DNA in base pairs, the apparent absorption coefficient  $\varepsilon_a$ ,  $\varepsilon_f$  and  $\varepsilon_b$  correspond to  $A_{\text{obs}}/[\text{compound}]$ , the extinction coefficient of the free compound and the extinction coefficient of the compound when fully bound to DNA, respectively. The plot of  $[\text{DNA}]/(\varepsilon_a - \varepsilon_f)$  versus [DNA] gave a slope and the intercept which are equal to  $1/(\varepsilon_b - \varepsilon_f)$  and  $1/K_b(\varepsilon_b - \varepsilon_f)$ , respectively;  $K_b$  is the ratio of the slope to the intercept. Plots of  $[\text{DNA}]/(\varepsilon_a - \varepsilon_f)$  versus [DNA] for the compounds with CT-DNA are shown in Fig. 3D. The magnitudes of intrinsic binding constants ( $K_b$ ) were calculated to be  $7.796 \times 10^4 \text{ M}^{-1}$ ,  $1.193 \times 10^5 \text{ M}^{-1}$  and  $1.712 \times 10^5 \text{ M}^{-1}$  corresponding to compounds **1**, **2** and **3**, respectively. The observed value of  $K_b$  revealed that the ligand and the Cu(II) complexes bind to DNA via intercalative mode [19,20]. And also, complex **3** is strongly bound with CT-DNA than that of **2** and **1** and the order of binding affinity is  $1 < 2 < 3$ . From the electronic absorption studies, though it has been found that the three compounds can bind to DNA by intercalation, the binding mode need to be proved through some more experiments.

**Table 2**  
Selected bond lengths (Å) and angles (°) for **2** and **3**.

	<b>2</b>	<b>3</b>
Cu(1)–O(1)	1.987(16)	1.942(3)
Cu(1)–N(1)	1.963(2)	1.952(3)
Cu(1)–O(2)	1.967(16)	1.952(3)
Cu(1)–Cl(2)	2.244(7)	
Cu(1)–O(3)	2.225(16)	
Cu(1)–O(35)		1.968(2)
Cu(1)–O(36)		2.262(4)
C(1)–N(1)	1.291(3)	1.290(3)
C(1)–C(2)	1.442(4)	1.466(3)
C(2)–C(3)	1.452(3)	1.470(3)
C(3)–O(1)	1.278(3)	1.271(3)
C(11)–O(2)	1.294(3)	1.300(3)
C(11)–N(2)	1.329(3)	1.333(3)
N(1)–N(2)	1.374(3)	1.395(2)
N(1)–Cu(1)–O(1)	90.78(7)	93.12(10)
O(2)–Cu(1)–O(1)	171.17(6)	174.00(6)
N(1)–Cu(1)–O(2)	80.45(7)	81.88(11)
O(2)–Cu(1)–O(3)	92.21(7)	
O(1)–Cu(1)–O(3)	91.01(6)	
N(1)–Cu(1)–O(3)	104.85(7)	
N(1)–Cu(1)–Cl(2)	155.54(6)	
O(2)–Cu(1)–Cl(2)	92.35(5)	
O(1)–Cu(1)–Cl(2)	95.29(5)	
O(3)–Cu(1)–Cl(2)	98.72(5)	
O(1)–Cu(1)–O(35)		88.15(11)
N(1)–Cu(1)–O(35)		162.11(8)
O(2)–Cu(1)–O(35)		95.60(12)
O(1)–Cu(1)–O(36)		93.81(10)
N(1)–Cu(1)–O(36)		96.50(10)
O(2)–Cu(1)–O(36)		90.06(10)
O(35)–Cu(1)–O(36)		101.22(12)
C(1)–N(1)–N(2)	116.8(2)	118.53(18)
C(1)–N(1)–Cu(1)	128.85(17)	128.06(13)
N(2)–N(1)–Cu(1)	114.21(14)	113.39(16)
C(11)–N(2)–N(1)	111.00(19)	110.43(18)
C(3)–O(1)–Cu(1)	127.88(16)	127.16(15)
C(11)–O(2)–Cu(1)	110.92(15)	110.14(15)
N(1)–C(1)–C(2)	124.2(2)	123.64(18)
O(2)–C(11)–N(2)	123.2(2)	124.01(18)
O(1)–C(3)–C(2)	124.5(2)	125.66(17)
C(1)–C(2)–C(3)	123.0(2)	122.20(18)

### 3.3.2. Fluorescence titration measurements

To further confirm the interactions between the studied compounds and CT-DNA, emission experiments were carried out. The H<sub>2</sub>L and the Cu(II) complexes exhibited weak luminescence in Tris–HCl buffer with a maximum wavelength of about 437 and 447 nm, when excited at 375 and 400 nm, respectively. The results of the emission titration for the complexes and the ligand with CT-DNA that are illustrated in the titration curves are shown in Fig. 4. The intensity of the emission for compounds **1**, **2** and **3** increased with the increase of DNA concentration. Upon the addition of CT-DNA, the emission intensities at 447 nm were increased by around 2.55 and 2.75 times for the complexes **2** and **3**, respectively. But, the emission intensity of the ligand (**1**) at 437 nm increased only around 1.63 times. This phenomenon is related to the extent to which the compound penetrates into the hydrophobic environment inside the DNA, thereby avoiding the quenching effect of solvent water molecules. The binding of complexes **2**, **3** and free ligand to CT-DNA leads to a marked increase in the emission intensity, which also agrees with those observed for other intercalators [34]. These results show that the complexes bind more strongly than the free ligand. From the observed intensity enhancement of the two complexes in the presence of CT-DNA, it can be seen that **3** has more DNA-binding ability than **2**. The higher binding affinity of the Cu(II) complexes is attributed to the extension of the  $\pi$  system of the intercalated ligand due to the coordination to Cu(II) ion. Since the complexes have greater planar area than that of the free ligand, enabling the complexes penetrating more deeply into, and stacking more strongly with the base pairs of the DNA.

### 3.3.3. Competitive binding between EB and the compounds for CT-DNA

Steady-state competitive binding experiments using the compounds **1**, **2** and **3** as quenchers were undertaken to get further proof for the binding of the compounds to DNA via intercalation. Ethidium bromide is a planar cationic dye which is widely used as a sensitive fluorescence probe for native DNA. EB emits intense fluorescent light in the presence of DNA due to its strong intercalation between the adjacent DNA basepairs [35,36]. The

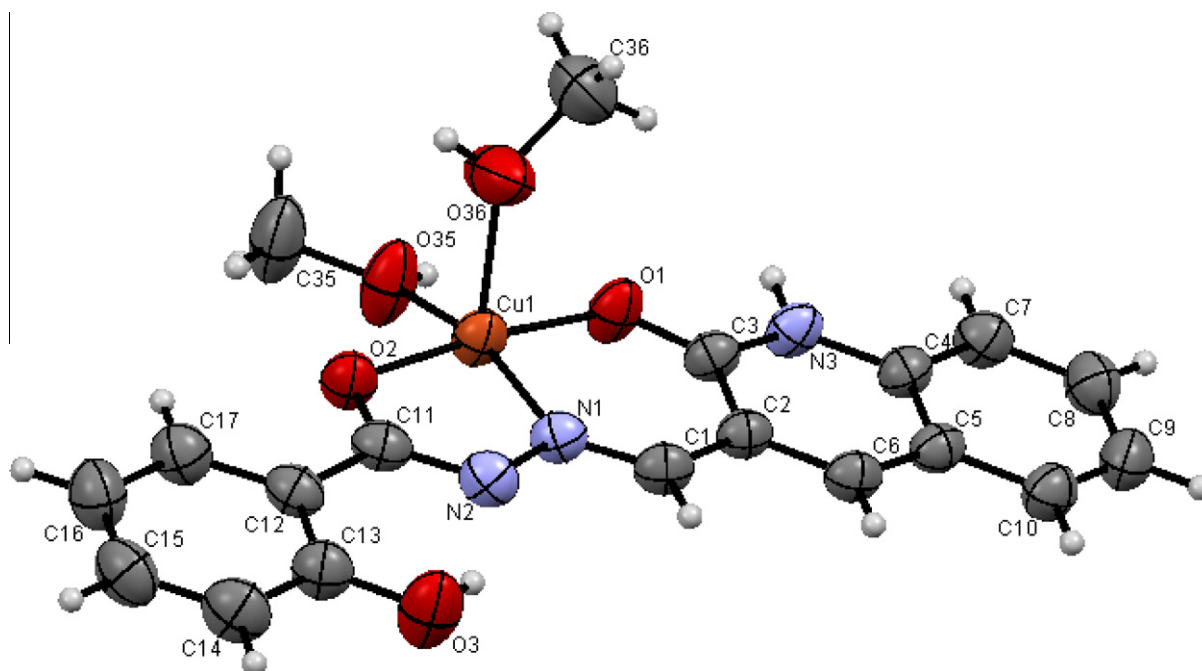


**Fig. 2.** ORTEP view of the molecular structure and atom-labeling scheme of **3**. Thermal ellipsoids are drawn at 50% probability level. The nitrate ion has been omitted for clarity.

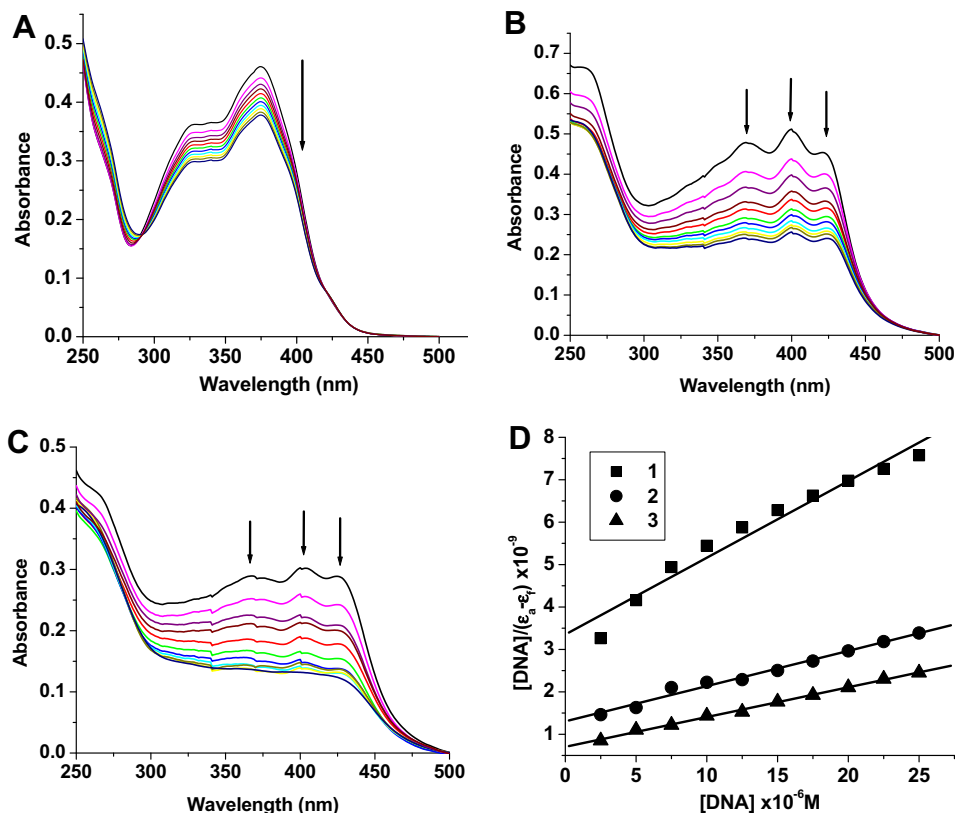


**Fig. 3.** Absorption spectra of compounds **1** (A), **2**(B) and **3** (C) (25  $\mu\text{M}$ ) in the presence of increasing amounts of CT-DNA (0, 2.5, 5, 7.5, 10, 12.5, 15, 17.5, 20, 22.5, and 25  $\mu\text{M}$ ; subsequent spectra). Arrows show the absorbance changes upon increasing DNA concentration. (D) Plots of  $[\text{DNA}]/(\epsilon_0 - \epsilon_t)$  versus  $[\text{DNA}]$  for the compounds with CT-DNA ( $K_b = 7.796 \times 10^4 \text{ M}^{-1}$ ,  $1.193 \times 10^5 \text{ M}^{-1}$  and  $1.712 \times 10^5 \text{ M}^{-1}$  corresponding to compounds **1**, **2** and **3**, respectively).

displacement technique is based on the decrease of fluorescence resulting from the displacement of EB from a DNA sequence by a quencher and the quenching is due to the reduction of the number of binding sites on the DNA that is available to the EB. The fluorescence quenching spectra of DNA-bound EB by compounds **1**, **2** and **3** shown in Fig. 5 illustrate that as the concentration of the compounds increases, the emission band at 602 nm exhibited hypochromism, up to 29.87%, 52.02% and 57.91% of the initial fluorescence intensity accompanied by a hypsochromic shift of 2, 3 and 5 nm for **1**, **2** and **3**, respectively. The observed decrease in the fluorescence intensity with a blue shift clearly indicates that the EB molecules are displaced from their DNA binding sites and are replaced by the compounds under investigation [37]. Quenching data were analyzed according to the following Stern–Volmer equation,

$$I_0/I = K_q[Q] + 1 \quad (3)$$

where  $I_0$  is the emission intensity in the absence of quencher,  $I$  is the emission intensity in the presence of quencher,  $K_q$  is the quenching constant, and  $[Q]$  is the quencher concentration. The  $K_q$  value is obtained as a slope from the plot of  $I_0/I$  versus  $[Q]$ .

The quenching plots illustrate that the quenching of EB bound to CT-DNA by **2**, **3** and free ligand (**1**) are in good agreement with the linear Stern–Volmer equation, which also proves that they bind to DNA. In the Stern–Volmer plots (Fig. 5D) of  $I_0/I$  versus  $[Q]$ , the quenching constant ( $K_q$ ) is given by the ratio of the slope to the intercept. The  $K_q$  values for **1**, **2** and **3** were  $1.075 \times 10^4 \text{ M}^{-1}$ ,  $2.757 \times 10^4 \text{ M}^{-1}$  and  $3.490 \times 10^4 \text{ M}^{-1}$ , respectively. Further, the binding constant ( $K_{\text{app}}$ ) values obtained for the compounds using the following equation,

$$K_{\text{EB}}[\text{EB}] = K_{\text{app}}[\text{compound}] \quad (4)$$

(where the compound concentration has the value at a 50% reduction of the fluorescence intensity of EB,  $K_{\text{EB}} = 1.0 \times 10^7 \text{ M}^{-1}$  and  $[\text{EB}] = 0.5 \mu\text{M}$ ) were  $8.190 \times 10^4 \text{ M}^{-1}$ ,  $1.278 \times 10^5 \text{ M}^{-1}$  and  $1.694 \times 10^5 \text{ M}^{-1}$  for **1**, **2** and **3**, respectively. These data suggested that the interaction of the copper(II) complexes with CT-DNA is stronger than that of the free ligand, which is consistent with the above absorption and emission spectral observations. Since these changes indicate only one kind of quenching process, it may be concluded that **1**, **2** and **3** bind to CT-DNA via the same mode. Furthermore, such quenching constants and binding constants of the ligand and Cu(II) complexes suggest that the interaction of all the compounds with DNA should be of intercalation [38]. On the basis of all the spectroscopic studies, we come to the conclusion that copper(II) complexes and free ligand can bind to CT-DNA in an intercalative mode and that the Cu(II) complexes bind to CT-DNA more strongly than the free ligand. Though the two copper(II) complexes have almost similar square pyramidal geometry, the cationic nature and the presences of two coordinated methanol molecules in **3** are likely to be the reason for the observed strong affinity of **3** with DNA over **2**.

### 3.4. Protein binding studies

#### 3.4.1. Fluorescence quenching of BSA by $\text{H}_2\text{L}$ and its two Cu(II) complexes

Serum albumin is the protein which increases the apparent solubility of drugs in plasma and modulates their delivery to cell. So, it is of important to understand the mechanism of interaction of a bioactive compound with protein. The nature and magnitude of drug–protein interaction influence the biological activity such as efficacy and delivery rate of the drug [39]. In addition, it is also important to study the binding parameters of drugs with protein

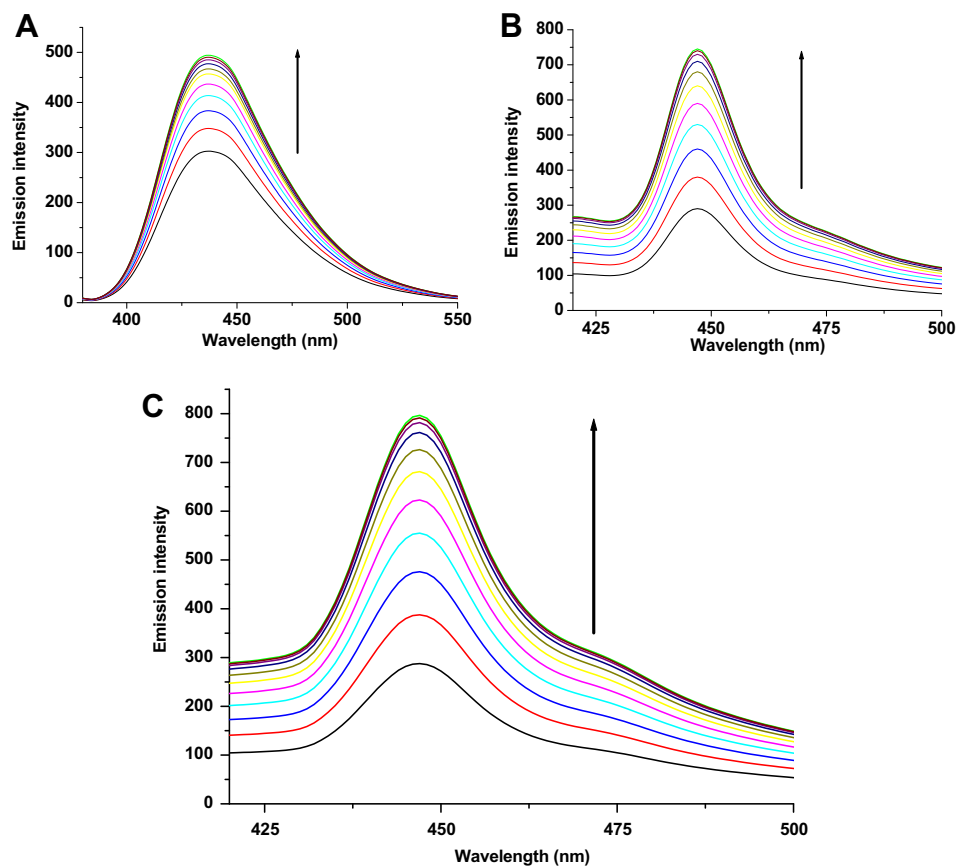


**Fig. 4.** Emission enhancement spectra of compounds **1** (A), **2**(B) and **3** (C) (25  $\mu\text{M}$ ) in the presence of increasing amounts of CT-DNA (0, 2.5, 5, 7.5, 10, 12.5, 15, 17.5, 20, 22.5, and 25  $\mu\text{M}$ ; subsequent spectra); arrow shows the emission intensity increases upon increasing DNA concentration.

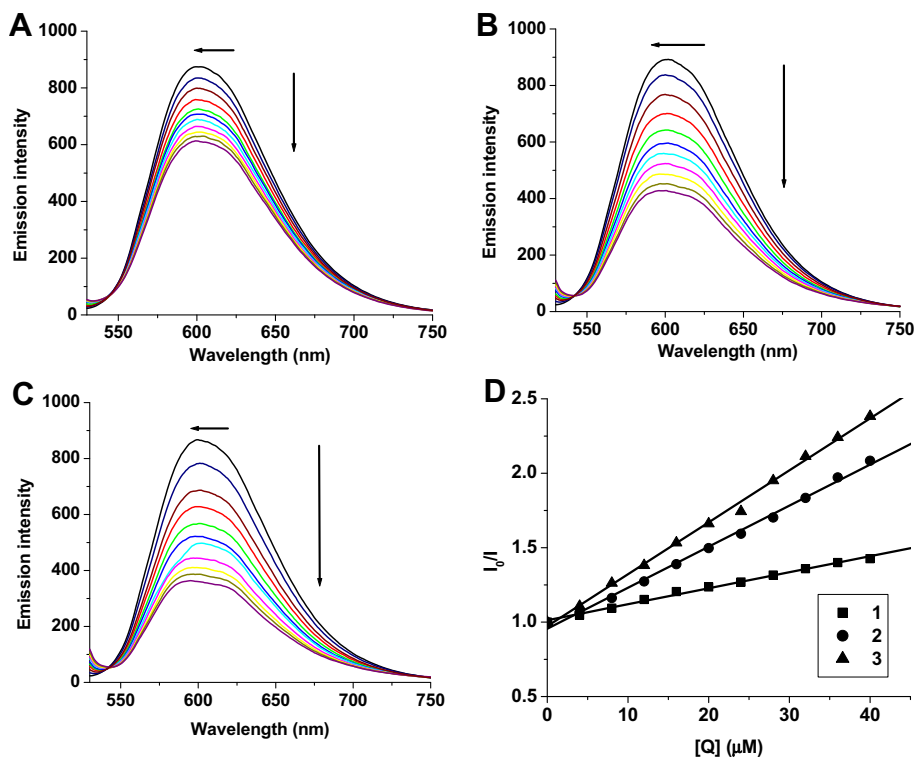


**Fig. 5.** Emission spectra of DNA-EB system (25  $\mu\text{M}$  DNA and 0.5  $\mu\text{M}$  EB),  $\lambda_{\text{ex}} = 510 \text{ nm}$ , in the presence of (0, 4, 8, 12, 16, 20, 24, 28, 32, 36, and 40  $\mu\text{M}$ ) **1** (A), **2** (B) and **3** (C). Arrows show the emission intensity changes upon increasing compounds concentration. (D) Stern-Volmer plots of the fluorescence titration of **1**, **2** and **3**. Quenching constant ( $K_q$ ) =  $1.075 \times 10^4 \text{ M}^{-1}$ ,  $2.757 \times 10^4 \text{ M}^{-1}$  and  $3.490 \times 10^4 \text{ M}^{-1}$  for **1**, **2** and **3**, respectively.

in order to control the pharmacological response of drugs and design of dosage forms. Serum albumin is considered as a model for studying drug–protein interaction *in vitro* since it is the major binding protein for drugs and other physiological substances. The analysis of chemical compounds bound to BSA has been carried out by examining the respective fluorescence spectra. Changes in molecular environment in the vicinity of fluorophore can be accessed by the changes in fluorescence spectra in the absence and presence of the compounds and hence, provide clues to the nature of the binding phenomenon. The interaction of our compounds with BSA protein was studied by fluorescence measurement at room temperature. A solution of BSA (1  $\mu\text{M}$ ) was titrated with various concentrations of the compounds (0–5  $\mu\text{M}$ ). Fluorescence spectra were recorded in the range of 290–440 nm upon excitation at 280 nm. The effect of compounds on the fluorescence emission spectrum of BSA is shown in Fig. 6. Addition of the compounds to the solution of BSA resulted in significant decrease of the fluorescence intensity of BSA at 346 nm, up to 42.78%, 54.23% and 56.67% of the initial fluorescence intensity of BSA accompanied by a hypsochromic shift of 4, 7 and 9 nm for **1**, **2** and **3**, respectively. The observed blue shift is mainly due to the fact that the active site in protein is buried in a hydrophobic environment. This result suggested a definite interaction of all the three compounds with the BSA protein. Quenching can occur by different mechanisms, which are usually classified as dynamic quenching and static quenching; dynamic quenching refers to a process in which the fluorophore and the quencher come into contact during the

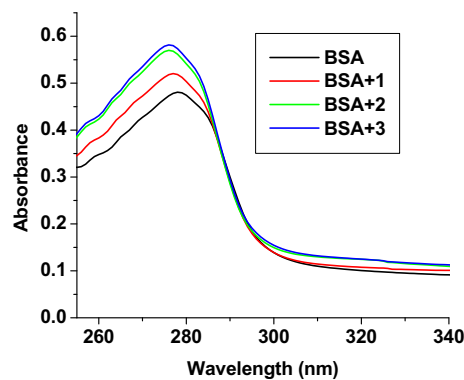


Fig. 7. Absorption spectra of BSA (10  $\mu\text{M}$ ) and with compounds, **1**, **2** and **3** (5  $\mu\text{M}$ ).

transient existence of the excited state. Static quenching refers to fluorophore–quencher complex formation in the ground state. A simple method to explore the type of quenching is UV–Vis absorption spectroscopy. UV–Vis spectra of BSA in the absence and presence of the compounds (Fig. 7) show that the absorption intensity of BSA was enhanced as the compounds were added, and there was a little blue shift of about 1, 2 and 2 nm for **1**, **2** and **3**, respectively. It revealed that there exists a static interaction between BSA and the added compounds due to the formation of ground state complex of the type BSA–compound as reported earlier [40]. To study

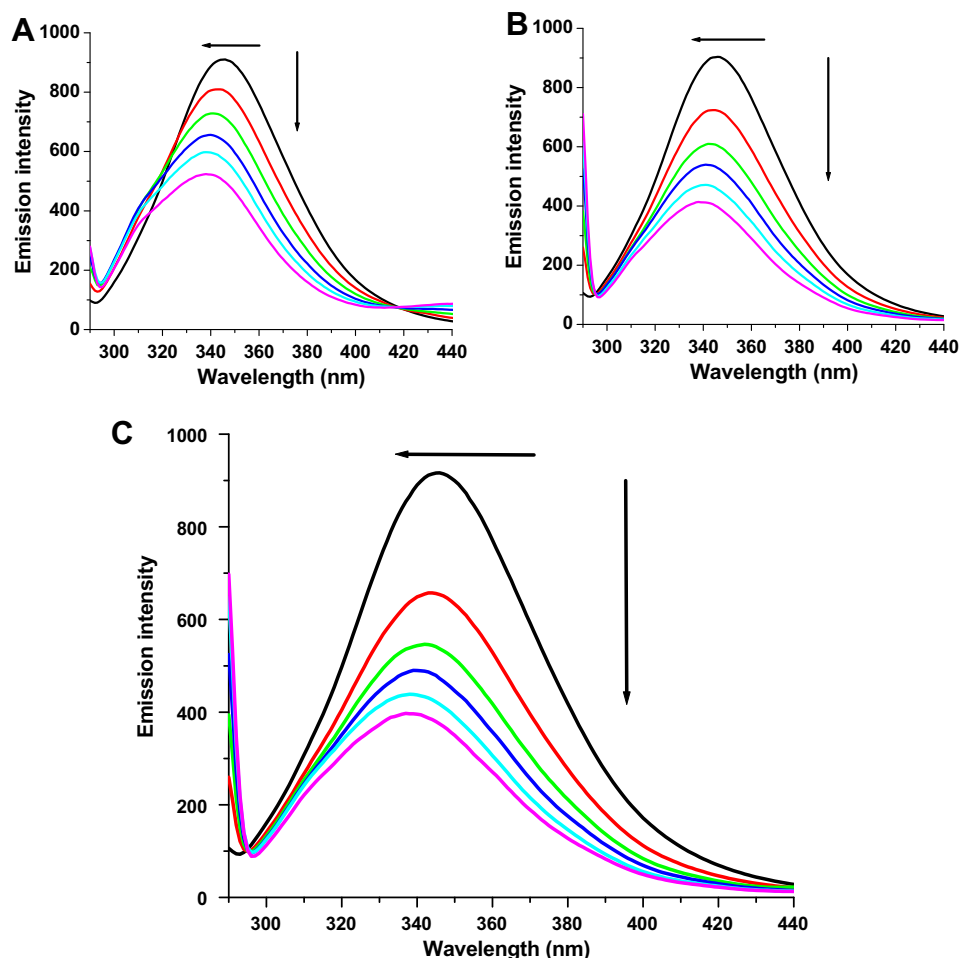
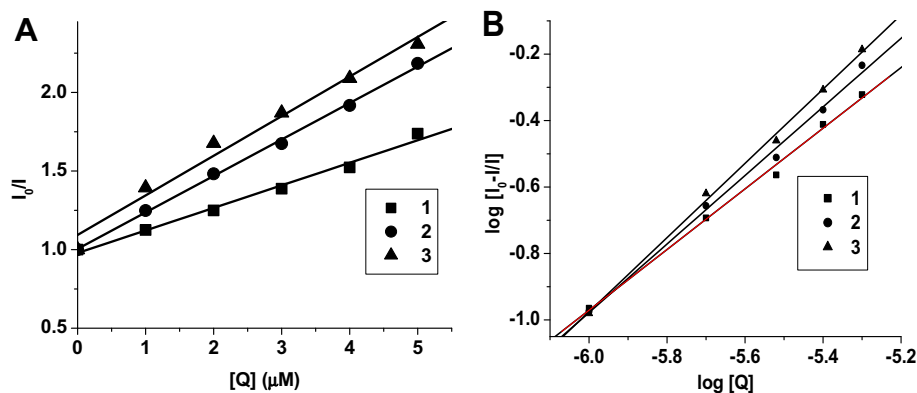


Fig. 6. The emission spectrum of BSA (1  $\mu\text{M}$ ;  $\lambda_{\text{exi}} = 280 \text{ nm}$ ;  $\lambda_{\text{emi}} = 346 \text{ nm}$ ) in the presence of increasing amounts of compounds **1** (A), **2** (B) and **3** (C) (0, 1, 2, 3, 4 and 5  $\mu\text{M}$ ). Arrow shows the fluorescence quenching upon increasing concentration of the compounds.



**Fig. 8.** (A) Stern-Volmer plots of the fluorescence titration of **1**, **2** and **3** with BSA. Quenching constant ( $K_q$ ) =  $1.435 \times 10^4 \text{ M}^{-1}$  (**1**),  $2.320 \times 10^5 \text{ M}^{-1}$  (**2**) and  $2.519 \times 10^5 \text{ M}^{-1}$  (**3**). (B) Scatchard plots of the fluorescence titration of **1**, **2** and **3** with BSA. Binding constant ( $K_{\text{bin}}$ ) =  $3.178 \times 10^4 \text{ M}^{-1}$  (**1**),  $1.456 \times 10^5 \text{ M}^{-1}$  (**2**) and  $1.858 \times 10^5 \text{ M}^{-1}$  (**3**).

**Table 3**

Quenching constant ( $K_q$ ), binding constant ( $K_{\text{bin}}$ ) and number of binding sites ( $n$ ) for the interactions of compounds with BSA.

Compound	$K_q \text{ (M}^{-1}\text{)}$	$K_{\text{bin}} \text{ (M}^{-1}\text{)}$	$n$
1	$1.435 \times 10^4$	$3.178 \times 10^4$	0.734
2	$2.320 \times 10^5$	$1.456 \times 10^5$	0.954
3	$2.519 \times 10^5$	$1.858 \times 10^5$	1.084

the quenching process further, fluorescence quenching data were analyzed with the Stern–Volmer equation (Eq. (3)) and Scatchard equation (Eq. (1)). The quenching constant ( $K_q$ ) can be calculated using the plot of  $I_0/I$  versus  $[Q]$  (Fig. 8A). From the plot of  $\log(I_0 - I)/I$  versus  $\log[Q]$  (Fig. 8B), the number of binding sites ( $n$ ) and binding constant ( $K_{\text{bin}}$ ) have been obtained. The calculated  $K_q$ ,  $K_{\text{bin}}$  and  $n$  values are given in Table 3. The calculated value of  $n$  is around one for all the compounds indicating the existence of just a single binding site in BSA for all the compounds. The value of  $K_q$  and  $K_{\text{bin}}$  for **1**, **2** and **3** suggested that the complexes interact with BSA more strongly than the ligand. Among the two square planar complexes, the cationic complex (**3**) which possesses two coordinated methanol has better interaction with BSA than the neutral complex (**2**).

#### 3.4.2. Characteristics of synchronous fluorescence spectra

To investigate the structural changes occurred to BSA upon the addition of our compounds, synchronous fluorescence spectra of BSA were measured before and after the addition of test compounds to get valuable information on the molecular microenvironment, particularly in the vicinity of the fluorophore functional groups [41]. It is a well-known fact that the fluorescence of BSA is normally due to the presence of tyrosine, tryptophan and phenylalanine residues and hence, spectroscopic methods are usually applied to study the conformation of serum protein. According to Miller [42], in synchronous fluorescence spectroscopy, the difference between excitation and emission wavelength ( $\Delta\lambda = \lambda_{\text{emi}} - \lambda_{\text{exi}}$ ) reflects the spectra of a different nature of chromophores. If the  $\Delta\lambda$  value is 15 nm, the synchronous fluorescence of BSA is characteristic of tyrosine residue where as a larger  $\Delta\lambda$  value of 60 nm is characteristic of tryptophan [43]. The synchronous fluorescence spectra of BSA with various concentrations of test compounds were recorded at  $\Delta\lambda = 15$  nm and  $\Delta\lambda = 60$  nm are shown in Figs. 9 and 10, respectively. In the synchronous fluorescence spectra of BSA at  $\Delta\lambda = 15$ , addition of the compounds to the solution of BSA resulted in a small decrease of the fluorescence intensity of BSA at 301 nm, up to 9.59%, 15.00% and 18.13% of the initial fluorescence intensity of BSA for **1**, **2** and **3**,

respectively. At the same time, in the case of synchronous fluorescence spectra of BSA at  $\Delta\lambda = 60$ , addition of the compounds to the solution of BSA resulted in significant decrease of the fluorescence intensity of BSA at 342 nm, up to 23.43%, 41.21% and 48.17% of the initial fluorescence intensity of BSA accompanied by a small blue shift of 2, 3 and 5 nm for **1**, **2** and **3**, respectively. The synchronous fluorescence spectral studies clearly suggested that the fluorescence intensities of both the tryptophan and tyrosine were decreased but the emission wavelength of the tryptophan residues is blue shifted with increasing concentration of compounds. At the same time, there is no change in the emission wavelength of tyrosine. It suggests that the interaction of compounds with BSA affects the conformation of tryptophan micro-region [21]. It reveals that the hydrophobicity around tryptophan residues is strengthened. The hydrophobicity observed in fluorescence and synchronous measurements confirmed the effective binding of all the compounds with the BSA. Hence, the strong interaction of these compounds with BSA suggested that the compounds may be fit for anticancer studies.

#### 3.5. Evaluation of radical scavenging ability

Since the experiments conducted so far revealed that the ligand and its Cu(II) complexes exhibit good DNA and protein binding affinity, it is considered worthwhile to study the antioxidant properties of these compounds. Radical scavenging activity is known to be one of the most important biological properties of metal complexes of quinoline derivatives, because they react with toxic free radicals and thus prevent damage to living organism. Moreover, our recent investigation suggested that there may be a relationship between the DNA/protein binding and the antioxidant properties of the compounds [37,38,44,45]. So the radical scavenging activities of our compounds along with standards, butylatedhydroxyanisole (BHA) and butylatedhydroxytoluene (BHT) in cell free system have been examined with reference to hydroxyl radicals, DPPH radicals, nitric oxide, superoxide anion radicals and the determination of  $\text{IC}_{50}$  values. It is to be noted that no significant radical scavenging activities were observed in all the experiments carried out with  $\text{CuCl}_2$  and  $\text{Cu}(\text{NO}_3)_2$ , even upto 1.0 mmol of concentration under the same experimental conditions. The  $\text{IC}_{50}$  values (Fig. 11) indicated that the three compounds showed antioxidant activity in the order of  $3 > 2 > 1$  in all the experiments. The DPPH radical scavenging power of the tested compounds was the most and super oxide anion radical scavenging was the least. These results are much better than that observed for standard antioxidants BHA and BHT. From the above results, it can be concluded that the scavenging effects of the free ligand is significantly less when compared to that of their corresponding Cu(II) complexes which

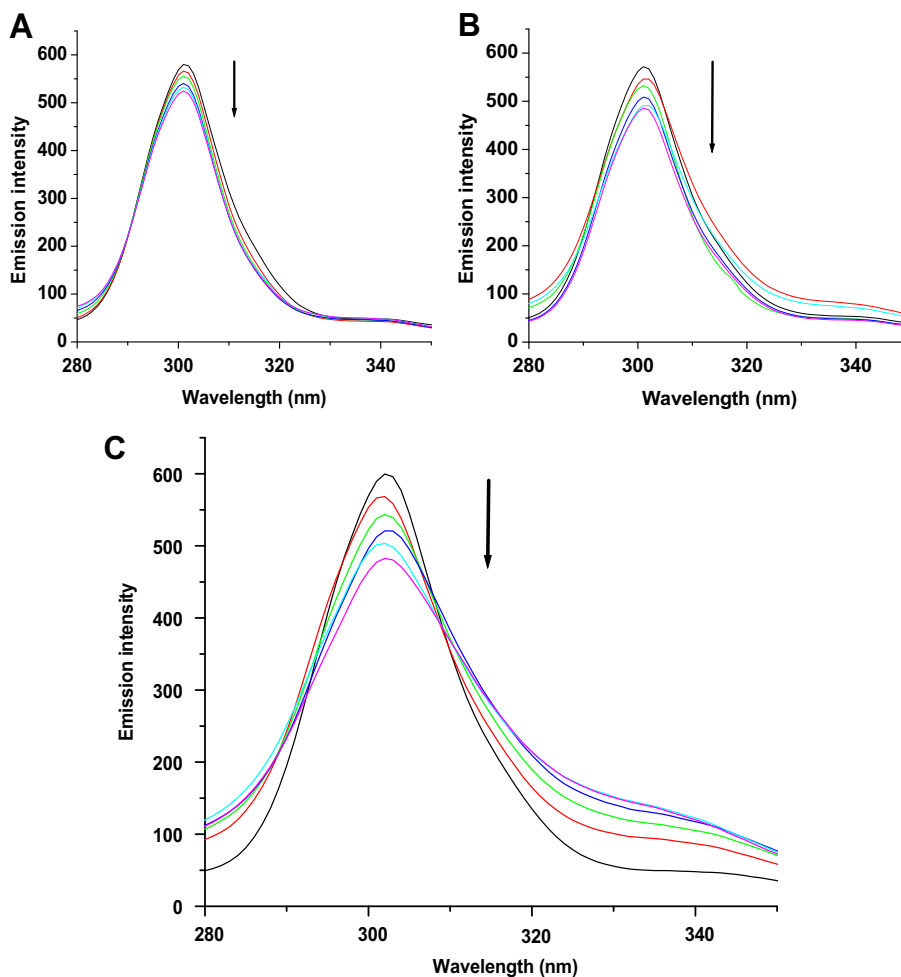


**Fig. 9.** Synchronous spectra of BSA (1  $\mu\text{M}$ ) in the presence of increasing amounts of compounds **1** (A), **2** (B) and **3** (C) (0, 1, 2, 3, 4 and 5  $\mu\text{M}$ ) in the wavelength difference of  $\Delta\lambda = 15$  nm. Arrow shows the emission intensity decrease upon the increasing concentration of compounds.

is due to the chelation of the organic ligand with the Cu(II) ion. Moreover, from the results obtained for the two Cu(II) complexes, it can be inferred that the difference in the nature of the complex and the co-ligands present in the complexes are likely to induce variations in antioxidant activities. Among the two complexes, the highest activity for **3** might be due to the presence of two coordinated methanol and cationic nature of the complex over the neutral square pyramidal complex (**2**).

### 3.6. Cytotoxic activity evaluation by MTT assay

The positive results obtained from the previous biological studies namely, DNA binding, BSA binding and antioxidative studies of **1**, **2** and **3** encouraged us to test their cytotoxicity against cancer cells. In order to understand the *in vitro* cytotoxicity of our compounds **1**, **2** and **3**, experiments were carried out using human cervical cancer cell line (HeLa) and normal mouse embryonic fibroblasts cell line (NIH 3T3). Compounds **1**, **2** and **3** were dissolved in DMSO and blank samples containing same volume of DMSO are taken as controls to identify the activity of solvent in this cytotoxicity experiment. Cisplatin was used as a standard to assess the cytotoxicity of compounds. The results were analyzed by means of cell viability curves and expressed as  $\text{IC}_{50}$  is shown in Fig. 12. The ligand did not show any significant activity even up to 200  $\mu\text{M}$  of concentration on HeLa cells. However, complexes **2** and **3** showed excellent activity on HeLa cells. The  $\text{IC}_{50}$  value of 23.67  $\mu\text{M}$  for **3** demonstrated a much higher

inhibitory effect than **2** (32.31  $\mu\text{M}$ ). The *in vitro* cytotoxic activity studies indicate that the two Cu(II) complexes have excellent activities against HeLa than the corresponding ligand but showed significantly less activity than cisplatin ( $\text{IC}_{50} = 9.42$   $\mu\text{M}$ ). In addition,  $\text{IC}_{50}$  values of all the compounds against NIH 3T3 mouse embryonic fibroblasts (normal cells) are found to be above 200  $\mu\text{M}$  which confirmed that the compounds are very specific on cancer cells. But, copper(II) chloride and copper(II) nitrate did not show any significant activity even up to 300  $\mu\text{M}$  of concentration on the HeLa cells which confirmed that the Cu(II) chelation with the ligand is the only responsible factor for the observed cytotoxic properties of the new complexes. The two Cu(II) complexes which possess better cytotoxic activities than ligand may be attributed to the extended planar structure induced by the  $\pi \rightarrow \pi^*$  conjugation resulting from the chelating of the metal ion with ligand. In addition, though both the Cu(II) complexes have square pyramidal geometry, the inhibitory rate of **3** against HeLa cancer cells is higher than **2** (Fig. 12), which may be due to the presence of two coordinated methanol and cationic nature of the complex [21].

## 4. Conclusion

A 2-oxo-1,2-dihydroquinoline-3-carbaldehyde(2'-hydroxybenzoyl)hydrazone and its two copper(II) complexes have been synthesized. Single crystal X-ray diffraction studies revealed that the both  $[\text{CuCl}(\text{HL})(\text{H}_2\text{O})]\cdot\text{CH}_3\text{OH}$  (**2**) and  $[\text{Cu}(\text{HL})(\text{CH}_3\text{OH})_2]\text{NO}_3$

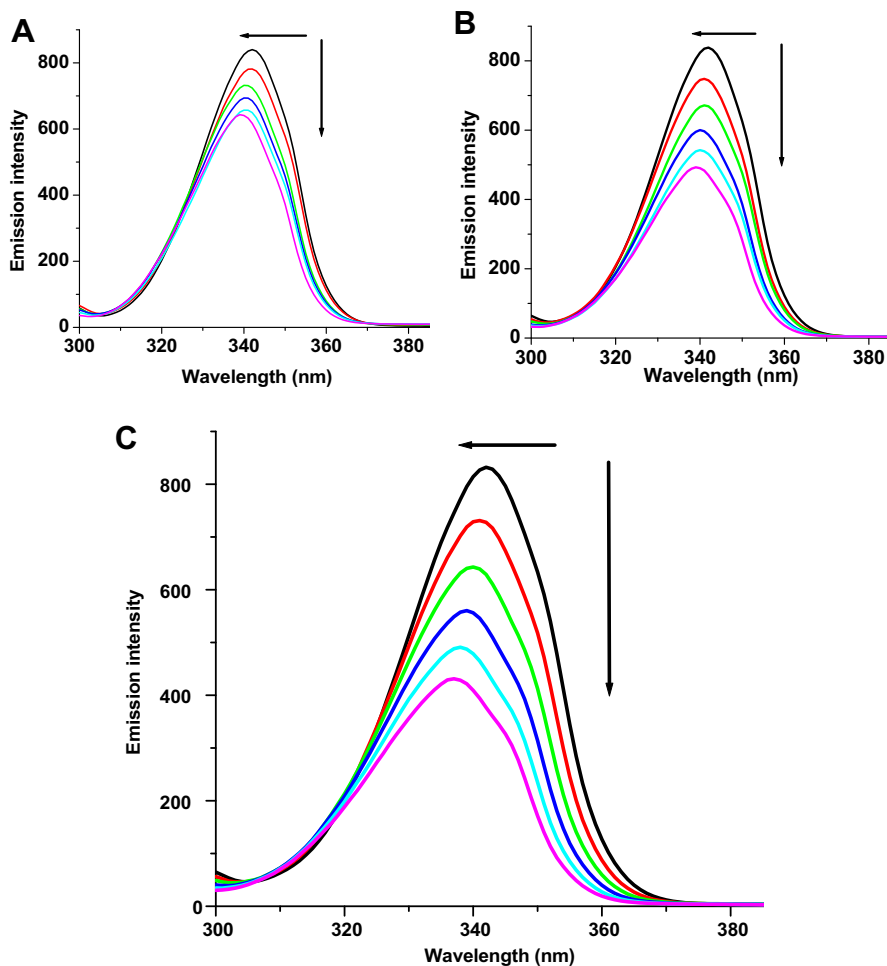


**Fig. 10.** Synchronous spectra of BSA (1  $\mu\text{M}$ ) in the presence of increasing amounts of compounds **1** (A), **2** (B) and **3** (C) (0, 1, 2, 3, 4 and 5  $\mu\text{M}$ ) in the wavelength difference of  $\Delta\lambda = 60$  nm. Arrows show the emission intensity changes upon the increasing concentration of compounds.

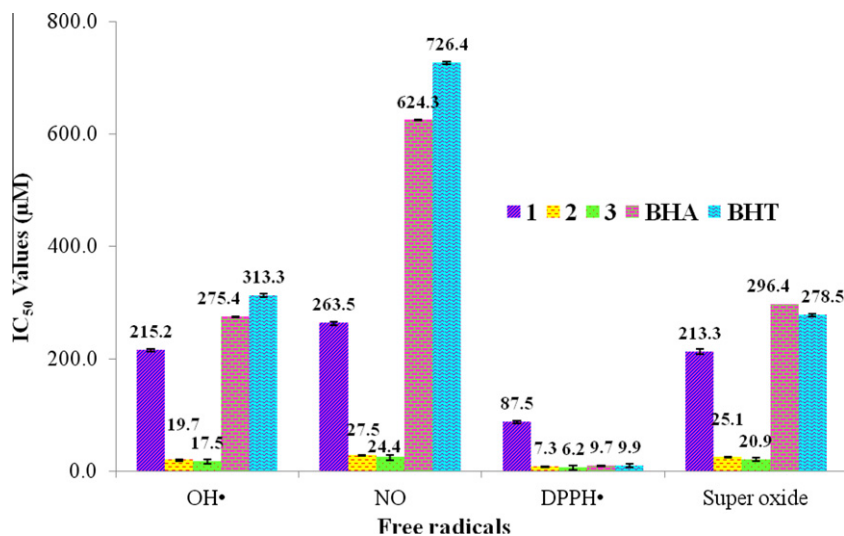


**Fig. 11.** Radical scavenging activity of the compounds.

**3**) have square pyramidal geometry with the ligand coordinating through uni-negative tridentate  $\text{ONO}^-$  fashion. The change of counter ion ( $\text{Cl}^-$  to  $\text{NO}_3^-$ ) in Cu(II) salts did not alter the coordination mode of ligand and the geometry of the resulted complexes. The DNA binding properties of the two Cu(II) complexes and the free ligand were investigated by absorption and fluorescence mea-

surements. The results supported the fact that the compounds bind to CT-DNA via intercalation. The binding constants show that the DNA binding affinity increased in the order  $1 < 2 < 3$ . Binding of the compounds with BSA monitored by UV-visible and fluorescence spectroscopy revealed the presence of static quenching and the results of synchronous spectral studies indicated that the com-

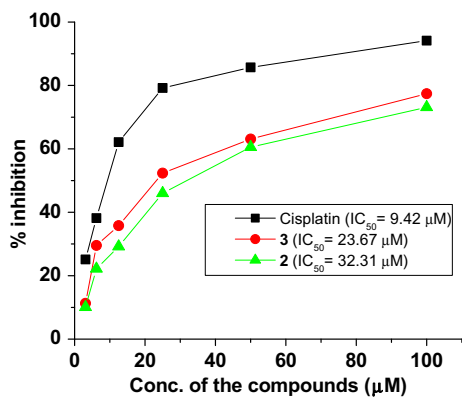


Fig. 12. Cytotoxic activity of compounds (cisplatin, **2** and **3**) against HeLa at various concentrations.

pounds bound with BSA mainly in tryptophan residues. In addition, the compounds also exhibited good antioxidant activities and the activity of **3** is better than that of **2** and **1**. The results of cytotoxicity study showed a linear relationship between the concentration of the Cu(II) complexes and the percentage inhibition of HeLa tumor cell growth without apparent damage to the normal cells. From the biological activity experiments, we observed that the cationic Cu(II) nitrate complex (**3**) which has two methanol molecules as co-ligands exhibited more potential than the neutral Cu(II) complex containing one water molecule and a chloride ion as co-ligands. So, overall, a structural dependent biological activity was observed which has been explained based on their structures. The findings are significant for us to explore further the DNA and protein interaction, antioxidative and cytotoxic activities of the transition metal complexes containing different 2-oxo-1,2-dihydroquinoline-3-carbaldehyde Schiff-bases.

#### Acknowledgment

Financial assistance received from the Council of Scientific and Industrial Research, New Delhi, India (Grant No. 01(2216)/08/EMR-II & 21(0745)/09/EMR-II), is gratefully acknowledged.

#### Appendix A. Supplementary data

Packing diagram of the unit cell showing hydrogen bonding of **2** and **3** has been given in Figs. S1 and S2, respectively. The hydrogen bonding parameters for **2** and **3** have been given in Tables S1 and S2, respectively. CCDC 825145 and 825268 contain the supplementary crystallographic data for complexes **2** and **3**, respectively. These data can be obtained free of charge from The Cambridge Crystallographic Data Centre via [www.ccdc.cam.ac.uk/data\\_request/cif](http://www.ccdc.cam.ac.uk/data_request/cif). Supplementary data associated with this article can be found, in the online version, at doi:10.1016/j.ica.2011.12.038.

#### References

- [1] V. Milacic, D. Chen, L. Ronconi, K.R. Landis-Piwowar, D. Fregona, Q.P. Dou, *Cancer Res.* 66 (2006) 10478.
- [2] I. Kostova, *Anticancer Agents Med. Chem.* 6 (2006) 19.
- [3] Z.A. Siddiqi, M. Khalid, S. Kumar, M. Shahid, S. Noor, *Eur. J. Med. Chem.* 45 (2010) 264.
- [4] S. Delaney, M. Pascaly, P.K. Bhattacharya, K. Han, J.K. Barton, *Inorg. Chem.* 41 (2002) 1966.
- [5] J. Tan, B. Wang, L. Zhu, *Bioorg. Med. Chem.* 17 (2009) 614.
- [6] B.P. Esposito, R. Najjar, *Coord. Chem. Rev.* 232 (2002) 137.
- [7] D.R. Green, J.C. Reed, *Science* 281 (1998) 1309.
- [8] Y. Ma, L. Cao, T. Kavabata, T. Yoshino, B.B. Yang, S. Okada, *Free Radical Biol. Med.* 25 (1998) 568.
- [9] F. Liang, C. Wu, H. Lin, T. Li, D. Gao, Z. Li, J. Wei, C. Zheng, M. Sun, *Bioorg. Med. Chem. Lett.* 13 (2003) 2469.
- [10] J. Easmon, G. Purstinger, G. Heinisch, T. Roth, H.H. Fiebig, W. Holzer, W. Jager, M. Jenny, J. Hofmann, *J. Med. Chem.* 44 (2001) 2164.
- [11] E.L. Hegg, J.N. Burstyn, *Coord. Chem. Rev.* 173 (1998) 133.
- [12] S. Dhar, D. Senapati, P.K. Das, P. Chattopadhyay, M. Nethaji, A.R. Chakravarty, *J. Am. Chem. Soc.* 125 (2003) 12118.
- [13] S. Dhar, P.A. Reddy, M. Nethaji, S. Mahadevan, M.K. Saha, A.R. Chakravarty, *Inorg. Chem.* 41 (2002) 3469.
- [14] P. Haskova, P. Kovarikova, L. Koubkova, A. Vavrova, E. Mackova, T. Simunek, *Free Radical Biol. Med.* 50 (2011) 537.
- [15] C.M. Moldovan, O. Oniga, A. Parvu, B. Tiperciuc, P. Verite, A. Pirnau, O. Crisan, M. Bojita, R. Pop, *Eur. J. Med. Chem.* 46 (2011) 526.
- [16] S. Banerjee, S. Mondal, S. Sen, S. Das, D.L. Hughes, C. Rizzoli, C. Desplanches, C. Mandal, S. Mitra, *Dalton Trans.* (2009) 6849.
- [17] S. Banerjee, S. Mondal, W. Chakraborty, S. Sen, R. Gachhui, R.J. Butcher, A.M.Z. Slawin, C. Mandal, S. Mitra, *Polyhedron* 28 (2009) 2785.
- [18] P. Krishnamoorthy, P. Sathyadevi, A.H. Cowley, R.R. Butorac, N. Dharmaraj, *Eur. J. Med. Chem.* 46 (2011) 3376.
- [19] Z.-C. Liu, B.-D. Wang, Z.-Y. Yang, Y. Li, D.D. Qin, T.-R. Li, *Eur. J. Med. Chem.* 44 (2009) 4477.
- [20] Z.-C. Liu, B.-D. Wang, B. Li, Q. Wang, Z.-Y. Yang, T.-R. Li, Y. Li, *Eur. J. Med. Chem.* 45 (2010) 5353.
- [21] D.S. Raja, G. Paramaguru, N.S.P. Bhuvanesh, J.H. Reibenspies, R. Renganathan, K. Natarajan, *Dalton Trans.* 40 (2011) 4548.
- [22] M.K. Singh, A. Chandra, B. Singh, R.M. Singh, *Tetrahedron Lett.* 48 (2007) 5987.
- [23] APEX2 and SAINT, Bruker AXS Inc., Madison, Wisconsin, USA.
- [24] G.M. Sheldrick, *Acta Crystallogr., Sect. A* 64 (2008) 112.
- [25] A.L. Spek, *Acta Crystallogr., Sect. D* 65 (2009) 148.
- [26] M.S. Blois, *Nature* 29 (1958) 1199.
- [27] T. Nash, *Biochem. J.* 55 (1953) 416.
- [28] L.C. Green, D.A. Wagner, J. Glogowski, P.L. Skipper, J.S. Wishnok, S.R. Tannenbaum, *Anal. Biochem.* 126 (1982) 131.
- [29] C. Beauchamp, I. Fridovich, *Anal. Biochem.* 44 (1971) 276.
- [30] J.K. Barton, A.T. Danishefsky, J.M. Goldberg, *J. Am. Chem. Soc.* 106 (1984) 2172.
- [31] S.M. Hecht, *J. Nat. Prod.* 63 (2000) 158.
- [32] M. Eriksson, M. Leijon, C. Hiort, B. Norden, A. Graeslund, *Biochemistry* 33 (1994) 5031.
- [33] A. Wolf, G.H. Shimer, T. Meehan, *Biochemistry* 26 (1987) 6392.
- [34] A. Nohara, T. Umetani, Y. Sanno, *Tetrahedron Lett.* 22 (1973) 1995.
- [35] F.J. Meyer-Almes, D. Porschke, *Biochemistry* 32 (1993) 4246.
- [36] G.M. Howe, K.C. Wu, W.R. Bauer, *Biochemistry* 19 (1976) 339.
- [37] D.S. Raja, N.S.P. Bhuvanesh, K. Natarajan, *Eur. J. Med. Chem.* 46 (2011) 4584.
- [38] D.S. Raja, N.S.P. Bhuvanesh, K. Natarajan, *J. Biol. Inorg. Chem.* (2011) doi:10.1007/s00775-011-0844-1.
- [39] B.P. Kamat, J. Seetharamappa, *J. Pharm. Biomed. Anal.* 35 (2008) 655.
- [40] X.Z. Feng, Z. Yang, L.J. Wang, C. Bai, *Talanta* 47 (1998) 1223.
- [41] G.Z. Chen, X.Z. Huang, Z.Z. Zheng, J.G. Xu, Z.B. Wang, *Methods of Fluorescence Analysis*, second ed., Science Press, Beijing, 1990.
- [42] J.N. Miller, *Proc. Anal. Div. Chem. Soc.* 16 (1979) 203.
- [43] J.H. Tang, F. Luan, X.G. Chen, *Bioorg. Med. Chem.* 149 (2006) 3210.
- [44] D.S. Raja, N.S.P. Bhuvanesh, K. Natarajan, *Eur. J. Med. Chem.* 47 (2012) 73.
- [45] D.S. Raja, N.S.P. Bhuvanesh, K. Natarajan, *Inorg. Chem.* 50 (2011) 12852.